Experimental Neurology 343 (2021) 113783

Contents lists available at ScienceDirect

Experimental Neurology

journal homepage: www.elsevier.com/locate/yexnr

Research paper

Cell-specific effects of *Dyt1* knock-out on sensory processing, network-level connectivity, and motor deficits

B.J. Wilkes [a,*], J.C. DeSimone [a], Y. Liu [b], W.T. Chu [a,c], S.A. Coombes [a], Y. Li [b], D. E. Vaillancourt [a,b,c]

[a] Department of Applied Physiology and Kinesiology, University of Florida, Gainesville, FL, USA
[b] Department of Neurology, University of Florida, Gainesville, FL, USA
[c] Department of Biomedical Engineering, University of Florida, Gainesville, FL, USA

ARTICLE INFO

Keywords:
Dystonia
Dyt1
torsinA
Sensorimotor
Dopamine-2 receptor
Cholinergic neurons
Cortex
Basal ganglia
Functional MRI
Diffusion MRI

ABSTRACT

DYT1 dystonia is a debilitating movement disorder characterized by repetitive, unintentional movements and postures. The disorder has been linked to mutation of the *TOR1A/DYT1* gene encoding torsinA. Convergent evidence from studies in humans and animal models suggest that striatal medium spiny neurons and cholinergic neurons are important in DYT1 dystonia. What is not known is how torsinA dysfunction in these specific cell types contributes to the pathophysiology of DYT1 dystonia. In this study we sought to determine whether torsinA dysfunction in cholinergic neurons alone is sufficient to generate the sensorimotor dysfunction and brain changes associated with dystonia, or if torsinA dysfunction in a broader subset of cell types is needed. We generated two genetically modified mouse models, one with selective *Dyt1* knock-out from dopamine-2 receptor expressing neurons (D2KO) and one where only cholinergic neurons are impacted (Ch2KO). We assessed motor deficits and performed *in vivo* 11.1 T functional MRI to assess sensory-evoked brain activation and connectivity, along with diffusion MRI to assess brain microstructure. We found that D2KO mice showed greater impairment than Ch2KO mice, including reduced sensory-evoked brain activity in key regions of the sensorimotor network, and altered functional connectivity of the striatum that correlated with motor deficits. These findings suggest that (1) the added impact of torsinA dysfunction in medium spiny and dopaminergic neurons of the basal ganglia generate more profound deficits than the dysfunction of cholinergic neurons alone, and (2) that sensory network impairments are linked to motor deficits in DYT1 dystonia.

1. Introduction

DYT1 dystonia is a neurological movement disorder expressed as repetitive, unintentional movements and disabling postures, often affecting most of the body (Albanese et al., 2013). The disorder has been linked almost exclusively to an in-frame ΔGAG mutation of the *TOR1A/DYT1* gene encoding the torsinA protein (Ozelius et al., 1997). Although there has been considerable work towards understanding the mechanisms underlying dystonia, there is a lack of understanding of how torsinA dysfunction effects specific cell types to generate the changes in motor function, sensory processing, and brain pathophysiology associated with dystonia. Understanding the *in vivo* changes in brain function and connectivity caused by a loss of torsinA function in specific cell types may provide crucial insight into the clinical and sensorimotor neurophysiological deficits of dystonia (Hallett, 1995; Martella et al., 2014, 2009; Quartarone and Hallett, 2013).

Convergent evidence from studies in humans and animal models provide evidence that medium spiny neurons and cholinergic interneurons of the striatum are important in the pathophysiology of DYT1 dystonia (Eskow Jaunarajs et al., 2019; Yokoi et al., 2011). Reduced striatal dopamine-2 receptor availability and binding have been reported in human *DYT1* mutation carriers (Asanuma et al., 2005; Carbon et al., 2009) and mice with the corresponding *Dyt1* +/ΔGAG mutation knocked-in (Dang et al., 2005), suggesting hypofunction of the indirect pathway. Similar dopamine-2 receptor hypofunction is observed in humans with focal dystonia (Berman et al., 2013; Simonyan et al., 2013). In addition, the dopamine-2 receptor agonist quinpirole has been shown to cause an excitation paradox of striatal cholinergic interneurons and a loss of muscarinic inhibition in mouse models (Dang et al., 2012; Martella et al., 2014, 2009; Pisani et al., 2006; Scarduzio

* Corresponding author at: Department of Applied Physiology and Kinesiology, University of Florida, P.O. Box 118205, Gainesville, FL 32611, USA.
E-mail address: bwilkes@ufl.edu (B.J. Wilkes).

https://doi.org/10.1016/j.expneurol.2021.113783
Received 25 March 2021; Received in revised form 4 June 2021; Accepted 8 June 2021
Available online 10 June 2021

et al., 2017; Sciamanna et al., 2012, 2011). Regarding cholinergic cells, *Dyt1* knock-in mice showed higher expression of mRNA for muscarinic receptor subtype M1 and lower mRNA for M4 receptors in the striatum (Richter et al., 2019). Moreover, the loss of striatal cholinergic interneurons has been observed in mice with conditional knock-out of *Dyt1* from forebrain GABAergic neurons (Pappas et al., 2015) and in mice with conditional knock-out of *Dyt1* from dopamine-2 receptor expressing cells (Yokoi et al., 2020).

In the present study, we sought to determine whether *Dyt1* dysfunction in cholinergic neurons alone would generate the sensorimotor dysfunction and brain changes associated with dystonia, or if torsinA dysfunction in a broader subset of basal ganglia cell types is needed. To accomplish this goal, we studied two genetically modified mouse models. In model 1, cell ftypes that express dopamine-2 receptors have conditional knock-out of *Dyt1* (D2KO), and this affects medium spiny neurons of the indirect pathway, striatal cholinergic interneurons, and dopaminergic neurons of the basal ganglia (Yokoi et al., 2020). These *Dyt1* D2KO mice were shown to have a reduced number of striatal cholinergic interneurons, acetylcholine metabolic enzymes, Tropomyosin receptor kinase A, striatal dopamine-2 receptor dimers, and demonstrate motor deficits in male mice (Yokoi et al., 2020). Evidence of indirect pathway hypofunction in humans with dystonia (Berman et al., 2013) and mouse models of dystonia (Dang et al., 2005) provide further rationale for studying brain changes in this D2KO model. In model 2, there is a conditional knock-out of *Dyt1* limited to only cholinergic neurons (Ch2KO; Liu et al., 2021). Compared to other *Dyt1* cholinergic KO models, a notable difference in the Ch2KO mouse model is that there is preservation of both Dyt1 alleles in non-targeted cells (Liu et al., 2021) rather than KO of a single *Dyt1* allele throughout the whole body and KO of both *Dyt1* alleles in targeted cholinergic cells (Pappas et al., 2015, 2018).

We compared sensory-evoked brain function and connectivity, and whole-brain microstructural changes, using *in vivo* functional MRI (fMRI) at 11.1 T in *Dyt1* D2KO and *Dyt1* Ch2KO mice. The rationale for using *in vivo* sensory-evoked fMRI is that there is prior clinical and neurophysiological evidence demonstrating somatosensory processing deficits in dystonia patients (Hallett, 1995). We evaluated whole-brain microstructure with diffusion imaging because this technique has shown promise in studying neurodegeneration in mouse models and humans (Burciu et al., 2017; Chu et al., 2020; Colon-Perez et al., 2019; DeSimone et al., 2017). We also assessed motor function in all animals using accelerated rotarod and beam walking assessments in order to determine whether imaging metrics correlated with motor deficits. Due to their numerous neurochemical deficits in the striatum, we hypothesized that D2KO mice would show deficient sensory-evoked striatal activation and functional connectivity compared to litter-mate controls. We also hypothesized that compared to litter-mate controls Ch2KO mice would show preserved striatal activation due to the limited proportion of total striatal cell types effected, but abnormal striatal connectivity due to the altered properties of cholinergic neurons in the striatum.

2. Materials and methods

2.1. Experimental design

This study included two cohorts of adult, male-only dystonia mouse models (D2KO and Ch2KO), each with their own respective litter-mate control group. We chose to perform this imaging investigation in male-only mice, as prior behavioral studies in several DYT1 dystonia mouse models found that only male mice had significant motor deficits (Dang et al., 2006, 2005; Yokoi et al., 2020). We used litter-mate control groups specific to each model in order to minimize the effects of background strain and cage-to-cage variability on comparisons of mutant *versus* control animals. Motor behavior assessment was performed on all animals and included accelerated rotarod and beam-walking tests. Three types of MRI scans were acquired for every animal: an anatomical scan, sensory-evoked fMRI, and diffusion MRI. Experimenters performing behavioral testing and magnetic resonance imaging were blind to which animals belonged to the experimental or control groups for each model. After all testing and data pre-processing was complete, animals were genotyped, and experimenters were unblinded in order to enable group-wise comparisons. Methods for each aspect of this study are described in detail in the following sections.

2.2. Animals

All experiments were performed in accordance with the National Institutes of Health guide for the care and use of Laboratory animals (NIH Publications No. 8023, revised 1978). The D2KO cohort included 21 mice with homozygous conditional knock-out of *Dyt1* specific to dopamine-2 receptor expressing neurons (mean age: 194.6 ± 26.6 d) and 22 *Dyt1* loxP +/− or *Dyt1* loxP −/− control mice (mean age: 194.2 ± 27.3 d). Generation of the D2KO mouse line has been previously described in detail (Yokoi et al., 2020). The Ch2KO cohort included 20 mice with homozygous conditional knock-out of *Dyt1* specific to cholinergic neurons (mean age: 180.6 ± 12.19) and 22 *Dyt1* loxP +/− or *Dyt1* loxP −/− control mice (mean age: 184.6 ± 10.91). Generation of the Ch2KO mouse line has been previously described in detail (Liu et al., 2021). Mice were maintained on a 12-h light/dark cycle with food and water *ad libitum*. All experiments were approved and monitored by the Institutional Animal Care and Use Committee at the University of Florida and were conducted in ethical compliance with the USPHS Guide for Care and Use of Laboratory Animals.

2.3. Motor behavior tests and analysis

Locomotor function was evaluated using accelerated rotarod (Ugo Basile) and beam-walking assessments as described previously (Yokoi et al., 2020). Rotarod and beam-walking tests respectively occurred 32.0 ± 13.9 d and 25.4 ± 13.6 d before D2KO imaging, and 29.7 ± 9.97 d and 34.33 ± 17.30 d before to Ch2KO imaging. For rotarod, mice were placed on a rotating spindle with an initial speed of 4 rpm and a gradual acceleration rate of 0.2 rpm/s. Latency-to-fall time was measured with a 180 s cutoff time and final speed of 40 rpm. Mice were tested across three separate trials each day for two consecutive days (6 total trials), with a 1 h inter-trial rest period. For beam-walking, mice were trained to traverse a medium size (14 mm width) square beam across three trials each day for two consecutive days (6 total training trials). Mice were evaluated on total beam slips across the two testing sessions. Day 3 included one testing trial traversing a medium square (14 mm width) and one trial traversing a medium round beam (17 mm diameter). Day 4 included one testing trial traversing a small square (7 mm width) and one trial traversing a small round beam (10 mm diameter). All beams were 100 cm in length and total beam slips were recorded for the middle 80 cm section. For both rotarod and beam-walking tests, group differences in latency-to-fall times and total beam slips were analyzed using the non-parametric GENMOD procedure in SAS (Dang et al., 2005).

2.4. MRI preparation

Mice were placed under general anesthesia for the duration of imaging. Initial knock-down occurred within an enclosed chamber under brief administration of 3% isoflurane delivered by compressed air through Surgivet vaporizer (Dublin, OH) connected to a charcoal trap. Anesthesia was maintained between 1 and 1.5% for the remaining experimental duration to accommodate necessary vitals and motion considerations. Research suggests that sensory neurons in the dorsal horn of the spinal cord that respond to noxious stimuli have relatively spared firing rates under isoflurane anesthesia (Kim et al., 2007). The experimental setup for mouse imaging is displayed in Fig. 1. Mice were placed in a prone position on a custom 3D printed mouse platform equipped with a bite-bar that immobilized the head and delivered

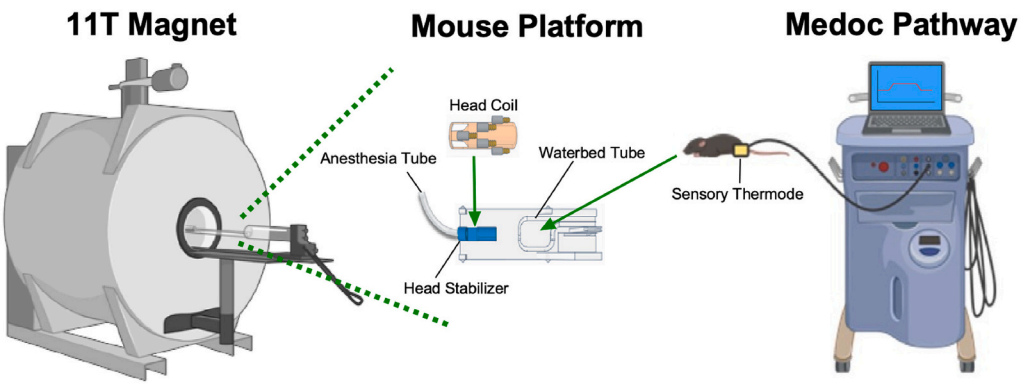

Fig. 1. Imaging setup. Imaging was performed on an 11.1 Tesla MRI scanner with a Magnex Scientific 40 cm horizontal magnet (Bruker BioSpin, Billerica, MA). For imaging, animals were placed on a custom-designed mouse platform, which included anesthesia provided through a head stabilizer with a surface transmit/receive radiofrequency head coil. Core body temperature was maintained during imaging with a heated waterbed tube placed underneath the animal. A Medoc PATHWAY heating thermode was placed on the right hindlimb of the animal and controlled by an associated computer setup.

anesthesia. Respiration was monitored using a respiration pad (SA Instruments, Stony Brook, NY) placed beneath the abdomen. Core body temperature was maintained using an in-house recirculating waterbed heating system and monitored *via* a thermal rectal probe (SA Instruments, Stony Brook, NY). A 256 mm^2 MR compatible advanced thermal stimulator (ATS) thermode (PATHWAY System, Medoc Advanced Medical Systems, Ramat Yishay, Israel) was affixed to right plantar hind paw, which delivered heat stimulation during imaging.

2.5. MRI acquisition

MRI data were acquired using an 11.1 Tesla Magnex Scientific 40 cm horizontal magnet (Agilent, Inc. Palo Alto, CA, USA) with RRI BFG-240/120-S6: bore size 120 mm, Gmax = 1000 mT/m @325A with 200 μs rise time. B^1 excitation and signal detection were achieved using an in-house 2.5 × 3.5 cm quadrature surface transmit/receive mouse head coil tuned to 470.7 MHz (^{1}H resonance) (AMRIS, University of Florida). Acquisition sequences were prepared and controlled using ParaVision, Version 6.0.1 (Bruker BioSpin, Billerica, MA).

Anatomical T2-weighted images were acquired for spatial normalization using a turbo RARE sequence with the following parameters: TR = 5500 ms; TE = 30 ms; excitation angle = 90°; refocusing angle = 180°; dummy scans = 1; averages = 7; slices = 13; orientation = coronal; thickness = 0.9 mm; gap = 0 mm; FOV = 15 × 15 mm; data matrix = 256 × 256 in-plane.

Two separate sensory-evoked fMRI runs were acquired using a 2-shot EPI sequence with the following parameters: TR = 2000 ms; TE = 15 ms; repetitions = 360; flip angle = 90°; dummy scans = 2; slices = 13; coronal orientation; thickness = 0.9 mm; gap = 0 mm; FOV = 15 × 15 mm; data acquisition matrix = 64 × 64 in-plane.

Acquisition of diffusion MRI data involved a two-shell HARDI protocol with the following parameters: TR = 4000 ms; TE = 19 ms; averages = 4; flip angle = 90°; slices = 17; orientation = coronal; thickness = 0.7 mm; gap = 0 mm; FOV = 15 × 11 mm; data matrix = 128 × 96 in-plane. The following diffusion parameters were used: two non-diffusion weighted b0 images; small shell b-value = 600 s/mm2; large shell b-value = 2000 s/mm2; directions = 52 total (six at b-value = 600 s/mm2; 46 at b-value = 2000 s/mm2).

2.6. Sensory-evoked fMRI thermal stimulation

Acquisition of sensory-evoked fMRI involved heat-induced stimulation of the right plantar hind paw. The PATHWAY System was calibrated such that thermal stimulation was applied in a block paradigm alternating between 60 s at the stimulation temperature (42 °C) and 60 s at the baseline temperature (30 °C), beginning and ending with a 30 s baseline block. The change in temperature between blocks was achieved within 300 ms *via* a cooling rate of 40 °C/s and a heating rate of 70 °C/s.

2.7. Sensory-evoked fMRI processing and analysis

Data processing and for sensory-evoked fMRI images were performed using custom-designed UNIX shell scripts in FMRIB Software Library (FSL: Oxford, UK) and Analysis of Functional NeuroImages (AFNI; Cox, 1996). Two separate analyses were performed: (1) examination of thermal stimulation induced blood-oxygen level dependent (BOLD) response and (2) a seed-based BOLD correlation analysis to examine functional connectivity in response to the thermal stimulation. Pre-processing for each sensory-evoked fMRI run included removal of five base volumes to account for magnetization equilibrium, rigid-body volume registration, spatial co-registration of the fMRI scan to the anatomical scan of each mouse, spatial warping of each scan to an anatomical template image, and in-plane spatial smoothing with a Gaussian full width at half-maximum (FWHM) kernel of 0.5 mm^2. Six head motion parameters (three rotational and three translational) were calculated and included as regressors of no-interest. The regression step also included censoring of consecutive functional volumes with more than 0.45 mm in relative motion. Six D2KO mutant and seven D2KO controls, as well as two of the controls in the Ch2KO cohort were, flagged for having high motion in more than 25% of total TRs and were removed from fMRI analyses. Processing for functional connectivity included an additional regressor of the mean CSF-related signal and bandpass filtering of the time series between 0.01 and 0.1 Hz.

To examine the sensory-induced BOLD activation response, the instantaneous BOLD signal at each voxel and each time-point was scaled by the average BOLD signal across its respective time-series for each mouse. The BOLD signals obtained from the baseline and stimulation blocks were modeled using a boxcar regressor convolved with a canonical hemodynamic response function. Using 3dDeconvolve in AFNI, the regression was performed across baseline and stimulation blocks to estimate the β-coefficient and its associated t-statistic for the BOLD contrast, separately for each run. Prior to investigating brain-wide differences in brain function and connectivity, we first compared sensory-evoked BOLD response in the hindlimb region of the primary somatosensory cortex using a region-of-interest (ROI) approach. ROIs for the left and right hindlimb region of primary somatosensory cortex were manually drawn according to The Mouse Brain in Stereotaxic Coordinates atlas (Paxinos and Franklin, 2nd edition). The mean β-coefficient for all voxels within the hindlimb ROI was compared using a 2 (group: mutant, control) by 2 (scan: 1,2) ANOVA. We then performed a whole-brain voxelwise ANOVA of β-coefficients using a 2 (group: mutant, control) by 2 (scan: 1, 2) design. In order to limit false-positives for the whole-brain analysis, a one-sample *t*-test in AFNI with *Clustsim* bootstrapping option was also performed on the control dataset from the first sensory-evoked fMRI scan to advise the cluster-extent threshold. In accordance with the advised threshold, between-group effects were considered significant ($p < 0.05$ FWER-corrected) at a minimum cluster size of 0.07 mm^3, for a *p*-value threshold of $p < 0.005$.

Functional connectivity was analyzed by examining the entire sensory-evoked fMRI time-series across baseline and stimulation blocks using a seed-based correlation approach, separately for each run. A total of 16 *a priori* selected seed regions-of-interest in the striatum were used in this analysis. Seeds were manually drawn on the template image in both the right and left striatum across two in-plane coronal slices (rostral and caudal striatum) in each of the dorsolateral, dorsomedial, ventrolateral, ventromedial quadrants. The selection of the striatum as the point of origin for seed-based connectivity was based on the hypothesis that knock-out of *Dyt1* from dopamine-2 receptor expressing cells (D2KO mice) and striatal cholinergic interneurons (Ch2KO mice) would disrupt sensorimotor networks of the striatum. Furthermore, a significant loss of striatal cholinergic interneurons has been observed in both models, suggesting a specific vulnerability of the striatum (Liu et al., 2021; Yokoi et al., 2020). After obtaining the residual time-series, Pearson's correlation coefficients were computed between the time-series of the seed and that of all other brain voxels, separately for each sensory-evoked fMRI run. Correlation coefficients were converted to *Z*-scores using Fisher r-to-z transformations. For the group-level analysis, Z-scores were analyzed using a 2 (group: mutant, control) by 2 (run: 1, 2) whole-brain voxelwise ANOVA, separately for each seed. Results were considered significant at a cluster-extent threshold of 0.05 mm^3 ($p <$ 0.05 FWER-corrected) based on the advised threshold for the BOLD activation analysis.

2.8. Diffusion MRI processing and analysis

Data processing for diffusion MRI was performed using custom-designed Unix shell scripts in FSL and AFNI. One D2KO and two corresponding control animals, as well as one Ch2KO animal were discarded due to high motion-related image distortion in the diffusion-weighted images. The processing pipeline included eddy-current and head motion correction, compensation of diffusion gradient rotations, and skull stripping of non-brain tissue. Next, calculation of voxelwise fractional anisotropy (FA) and mean diffusivity (MD) maps was performed using DTIFIT in FSL. The fitted FA map for each mouse was non-linearly warped to a standard FA template using the ANTs toolbox (Avants et al., 2010) and the resultant transformation matrix was applied to the MD map.

Group-level FA and MD effects between mutant and control animals were examined using two separate approaches. In the first analysis, FA and MD differences were examined using whole-brain independent-samples *t*-tests between mutant animals (D2KO, Ch2KO) and their respective control counterparts. These voxelwise t-tests were carried out using Randomise, a statistical analysis tool in FSL, with 1000 permutations and threshold-free cluster enhancement (TFCE; Smith and Nichols, 2009). In the second analysis, independent-samples t-tests were performed in R to examine the difference in mean FA and MD values with a set of specific regions-of-interest (ROI) selected *a priori* based on their relevance to DYT1 dystonia: striatum, sensorimotor cortex, thalamus, midbrain, pons, anterior medulla, posterior medulla, cerebellar cortex, and cerebellar vermis. Group effects were considered significant at $p <$ 0.05 FDR-corrected.

2.9. Correlation between behavior and sensory-evoked fMRI

Spearman rank correlations were carried out separately for each mutant cohort using Graphpad Prism (Version 8.4.1) to determine the relation between locomotor function and imaging outcomes. Significant between-group activation and connectivity clusters from the ANOVA analyses were masked to respectively compute mean β-coefficient and *Z*-score values for each mouse. Mean β-coefficient and Z-score values were then averaged across both sensory-evoked fMRI runs, resulting in a single value for each. β-coefficient and Z-score values were tested against average latency-to-fall times across the six trials in the rotarod assessment and total beam slips across the four total trials for the small round and square beams. The medium-sized beams yielded insufficient slips and thus were not included in this correlation analysis to avoid floor effects. We FDR-corrected for each voxel cluster in relation to behavioral tasks. BOLD activation and connectivity clusters were examined independently for each behavioral task.

3. Results

3.1. Motor behavior

The D2KO cohort demonstrated significantly reduced average latency-to-fall during rotarod ($p = 0.039$) and a significant increase in average beam-walking slips ($p = 0.042$) compared to controls (Fig. 2). The Ch2KO mice did not significantly differ from controls in rotarod or beam-walking performance (Fig. 2).

3.2. BOLD activation in D2KO and Ch2KO mice

To evaluate if sensory processing was occuring normally from spinal cord to somatosensory cortex, we quantified the hindlimb region BOLD signal corresponding to the sensory-evoked event. BOLD activity in the hindlimb region of the primary somatosensory cortex was preserved as there was no difference in either D2KO (Left, $p = 0.24$; Right, $p = 0.76$) or Ch2KO (Left, $p = 0.56$; Right, $p = 0.89$) mice, compared to littermate their controls. Subsequent whole-brain voxelwise analysis revealed that D2KO mice had reduced BOLD activation compared to control mice in regions including striatum, globus pallidus, sensorimotor cortex, associative cortex, and thalamus ($p < 0.05$ FWER-corrected; Fig. 3). We observed no significant effect of scan number (1 or 2), suggesting that the average BOLD signal across both sensory-evoked fMRI scan repetitions were robust in D2KO mice. In Ch2KO mice, BOLD activation was reduced compared to controls in a single midbrain cluster ($p < 0.05$ FWER-corrected; Fig. 4). We did observe a significant effect of scan in the Ch2KO cohort ($p < 0.05$), but there was no interaction between scan and group, suggesting that any effects were evenly distributed between

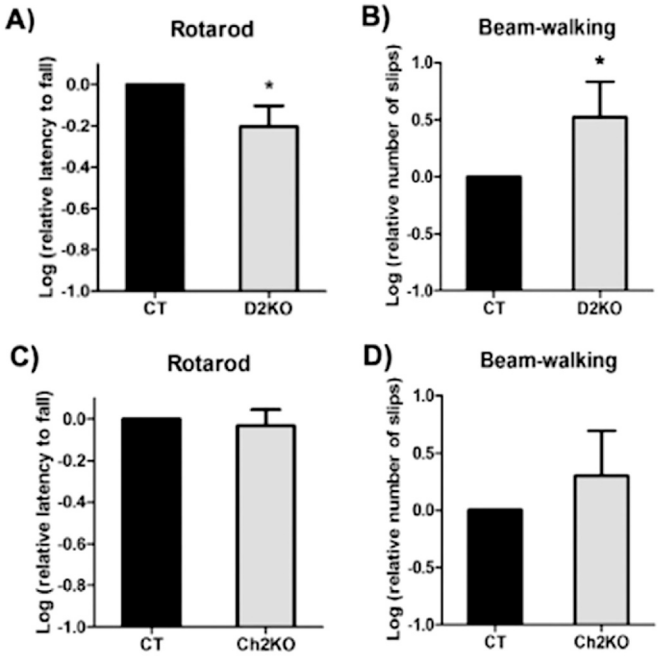

Fig. 2. Motor performance in D2KO and Ch2KO mice. The top panel (A–B) shows rotarod and beam-walking behavior analysis for D2KO model, both of which showed significant deficits (*$p < 0.05$). The bottom panel (C–D) shows rotarod and beam-walking behavior analysis for Ch2KO model, which did not show a significant difference from controls.

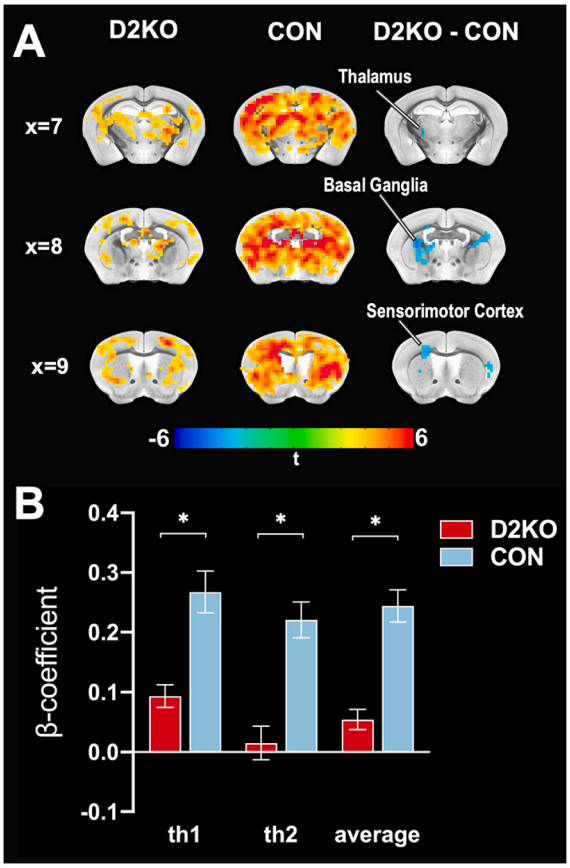

Fig. 3. D2KO Sensory-evoked BOLD. (A) Coronal slices representing BOLD signal response to thermal stimulation in D2KO (left column) and CON (middle column) animals. Significant group differences in BOLD response are shown in the right column ($p < 0.05$ FWER-corrected). Colored voxels indicate *t*-test values. (B) Bar graphs depicting mean (± standard error) B-coefficient values across voxels that showed a significant group difference between D2KO (red) and CON animals (blue). (For interpretation of the references to colour in this figure legend, the reader is referred to the web version of this article.)

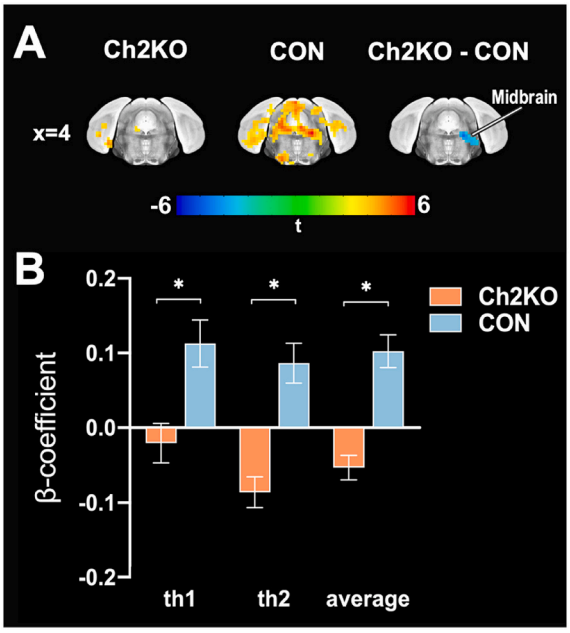

Fig. 4. Ch2KO Sensory-evoked BOLD. (A) Coronal slices representing BOLD signal response to thermal stimulation in Ch2KO (left column) and CON (middle column) animals. Significant group differences in BOLD response are shown in the right column ($p < 0.05$ FWER-corrected). Colored voxels indicate t-test values. (B) Bar graphs depicting mean (± standard error) B-coefficient values across voxels that showed a significant group difference between Ch2KO (orange) and CON animals (blue). (For interpretation of the references to colour in this figure legend, the reader is referred to the web version of this article.)

mutant and control animals in the Ch2KO cohort.

3.3. Functional connectivity in D2KO and Ch2KO mice

In D2KO mice compared to controls, there was reduced functional connectivity between the right ventrolateral striatum seed and two clusters in the left striatum and sensory cortex, as well as reduced functional connectivity between the left ventromedial striatum seed on slice 10 (anterior) and a cluster in the right striatum, as well as the left ventromedial striatum seed on slice 9 (posterior) and a cluster that extends across right striatum and piriform cortex area ($p < 0.05$ FWER-corrected; Fig. 5). In Ch2KO mice compared to controls, there was increased functional connectivity between the right dorsomedial striatum seed on slice 10 and a cluster in the right cerebellar cortex, as well as the left ventrolateral striatum seed on slice 9 and a cluster in left sensorimotor cortex ($p < 0.05$ FWER-corrected; Fig. 6).

3.4. No diffusivity changes in mutant mice

For the whole-brain voxelwise analysis of FA and MD, we found no evidence of between-group differences for either D2KO or Ch2KO mice compared to controls. Similarly, we found that neither D2KO nor Ch2KO mice had significant differences in FA or MD for the ROI-based analysis compared to controls (Table 1).

3.5. Correlations between imaging and behavior

In behavioral metrics where we found a group difference between KO and control mice, we also sought to investigate whether motor deficits correlated with sensory-evoked fMRI. In the D2KO cohort, mutant animals demonstrated an inverse correlation where an increased number of beam slips was associated with reduced BOLD signal in a cluster spanning the right striatum, globus pallidus, and sensory and associative cortices, $r = -0.56$, $p = 0.033$. Mutant D2KO animals also demonstrated an inverse correlation, where longer rotarod latency-to-fall was associated with reduced functional connectivity in a cluster in the left striatum (seed: right ventrolateral striatum, slice 1), $r = -0.56$, $p = 0.034$. Although no significant differences in motor performance were observed in this cohort of Ch2KO mutant mice, we did observe a significant negative correlation, where shorter rotarod latency-to-fall was correlated with greater functional connectivity of the right striatum to cerebellum (seed: right dorsomedial striatum, slice 1), $r = -0.57$, $p = 0.0081$. There were no significant brain-behavior correlations for the control animals in either D2KO or Ch2KO cohorts.

4. Discussion

The pathophysiology of DYT1 dystonia is strongly linked to basal ganglia dysfunction, particularly medium spiny neurons and cholinergic interneurons of the striatum (Eskow Jaunarajs et al., 2019; Yokoi et al., 2020, 2011). Despite their critical role, little is known about how torsinA dysfunction in these cell types specifically contributes to abnormal sensorimotor network function in DYT1 dystonia. In the present study, we sought to determine whether *Dyt1* dysfunction in cholinergic neurons alone would generate the sensorimotor dysfunction and brain changes associated with dystonia, or if torsinA dysfunction in a broader subset of dopamine-2 receptor expressing cell types was needed. We found that D2KO mice showed motor deficits, reduced sensory-evoked brain activity, and altered functional connectivity of the striatum

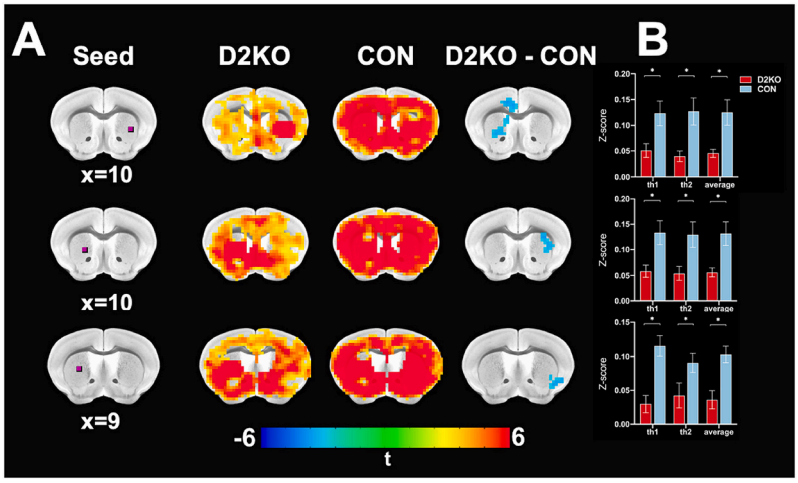

Fig. 5. D2KO Striatal Functional Connectivity. (A) Coronal slices representing functional connectivity from seed regions in the striatum (first column) for D2KO (second column) and CON (third column) animals. Significant group differences in BOLD response are shown in the fourth column ($p < 0.05$ FWER-corrected). Colored voxels indicate t-test values. (B) Bar graphs depicting mean (± standard error) *Z*-score values across voxels that showed a significant group difference between D2KO (red) and CON animals (blue). Only seeds where a significant difference was found between groups are shown, including the right ventrolateral striatum seed on slice 10 (top row), left ventromedial striatum seed on slice 10 (middle row), and left ventromedial striatum seed on slice 9 (bottom row). (For interpretation of the references to colour in this figure legend, the reader is referred to the web version of this article.)

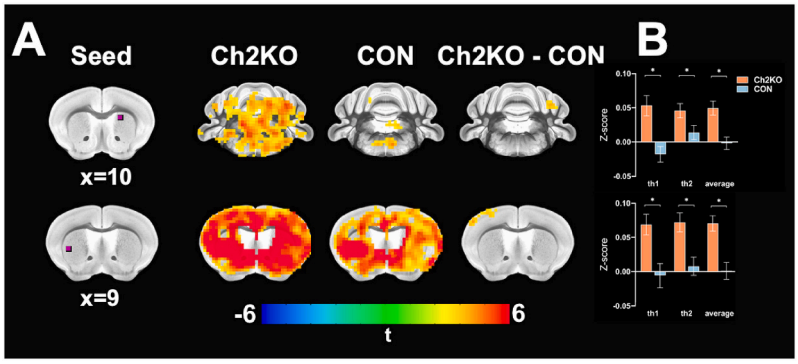

Fig. 6. Ch2KO Striatal Functional Connectivity. (A) Coronal slices representing functional connectivity from seed regions in the striatum (first column) for Ch2KO (second column) and CON (third column) animals. Significant group differences in BOLD response are shown in the fourth column ($p < 0.05$ FWER-corrected). Colored voxels indicate t-test values. (B) Bar graphs depicting mean (± standard error) Z-score values across voxels that showed a significant group difference between Ch2KO (orange) and CON animals (blue). Only seeds where a significant difference was found between groups are shown, including the right dorsomedial striatum seed on slice 10 (top row) and left ventrolateral striatum seed on slice 9 (bottom row). (For interpretation of the references to colour in this figure legend, the reader is referred to the web version of this article.)

Table 1
Region of interest analysis of diffusion MRI metrics (Welch's t-test) for D2KO (A) and Ch2KO (B) genetic model studies. Left column contains results for mean diffusivity (MD) and right column contains results for fractional anisotropy (FA).

(A) D2KO Study								
	Mean diffusivity (MD)				Fractional anisotropy (FA)			
	D2KO Group mean ± StDev	D2Control Group mean ± StDev	Pval	FDR-Pval	D2KO Group mean ± StDev	D2Control Group mean ± StDev	Pval	FDR-Pval
Cerebellum	5.564 ± 0.294 E-04	5.664 ± 0.222E-04	0.249	0.315	0.197 ± 0.045	0.193 ± 0.023	0.732	0.921
Vermis	5.599 ± 0.32 E-04	5.789 ± 0.241E-04	0.052	0.163	0.193 ± 0.045	0.194 ± 0.026	0.906	0.921
aMedulla	5.784 ± 0.297E-04	5.902 ± 0.275E-04	0.216	0.315	0.207 ± 0.038	0.208 ± 0.025	0.921	0.921
pMedulla	5.716 ± 0.293E-04	5.905 ± 0.271E-04	0.049	0.163	0.213 ± 0.033	0.223 ± 0.028	0.349	0.921
Pons	5.793 ± 0.269E-04	5.955 ± 0.249E-04	0.065	0.163	0.226 ± 0.024	0.231 ± 0.018	0.421	0.921
Midbrain	5.713 ± 0.216E-04	5.851 ± 0.238E-04	0.073	0.163	0.250 ± 0.020	0.253 ± 0.017	0.740	0.921
Thalamus	6.086 ± 0.237E-04	6.168 ± 0.221E-04	0.280	0.315	0.199 ± 0.013	0.200 ± 0.013	0.855	0.921
SS	6.086 ± 0.320E-04	6.138 ± 0.250E-04	0.360	0.360	0.153 ± 0.029	0.151 ± 0.024	0.837	0.921
Striatum	5.784 ± 0.20 E-04	5.873 ± 0.227E-04	0.214	0.315	0.199 ± 0.024	0.192 ± 0.029	0.451	0.921
(B) Ch2KO Study								
	Mean diffusivity (MD) Ch2KO	Ch2Control	Pval	FDR-Pval	Fractional anisotropy (FA) Ch2KO	Ch2Control	Pval	FDR-Pval
Cerebellum	5.378 ± 0.258E-04	5.474 ± 0.252E-04	0.250	0.376	0.175 ± 0.023	0.169 ± 0.016	0.352	0.883
Vermis	5.382 ± 0.307E-04	5.425 ± 0.356E-04	0.689	0.689	0.169 ± 0.034	0.168 ± 0.025	0.883	0.883
aMedulla	5.735 ± 0.226 E-04	5.866 ± 0.184E-04	0.055	0.376	0.177 ± 0.028	0.174 ± 0.022	0.733	0.883
pMedulla	5.552 ± 0.292E-04	5.678 ± 0.272E-04	0.173	0.376	0.191 ± 0.030	0.183 ± 0.023	0.345	0.883
Pons	5.660 ± 0.195E-04	5.735 ± 0.248E-04	0.299	0.376	0.216 ± 0.020	0.214 ± 0.023	0.799	0.883
Midbrain	5.585 ± 0.234E-04	5.667 ± 0.245E-04	0.294	0.376	0.246 ± 0.019	0.245 ± 0.015	0.811	0.883
Thalamus	5.912 ± 0.202E-04	6.035 ± 0.242E-04	0.095	0.376	0.198 ± 0.013	0.195 ± 0.012	0.492	0.883
SS	5.871 ± 0.206E-04	5.937 ± 0.214E-04	0.334	0.376	0.127 ± 0.027	0.121 ± 0.022	0.446	0.883
Striatum	5.622 ± 0.168E-04	5.686 ± 0.182E-04	0.262	0.376	0.185 ± 0.027	0.174 ± 0.016	0.139	0.883

Mean ± standard deviation, *p*-value, and false discover rate (FDR) corrected *p*-values are reported.
Abbreviations: anterior medulla (aMedulla); posterior medulla (pMedulla), sensorimotor cortex (SS).

compared to littermate controls, and that striatal connectivity changes correlated with motor deficits in KO mice. In contrast Ch2KO mice had fewer differences compared to litter-mate controls, with no significant differences in motor behavior or sensory-evoked brain activity, although altered functional connectivity between the striatum and cerebellum was observed. These findings suggest that (1) the added impact of torsinA dysfunction in medium spiny and dopaminergic neurons of the basal ganglia generate more profound deficits than the dysfunction of cholinergic neurons alone, and (2) that sensory network impairments are linked to motor deficits in DYT1 dystonia.

In D2KO mice cell types that express dopamine-2 receptors have conditional knock-out of *Dyt1* and include medium spiny neurons of the indirect pathway, striatal cholinergic interneurons, and dopaminergic neurons of the basal ganglia (Yokoi et al., 2020). During sensory-evoked fMRI, D2KO mice had lower BOLD signal compared to controls in regions of the basal ganglia network, including the striatum, globus pallidus, thalamus, and cortex. The Ch2KO model, in contrast, has conditional knock-out of *Dyt1* limited to cholinergic neurons (Liu et al., 2021) and only showed reduced BOLD signal in the midbrain compared to controls. A notable difference in the Ch2KO mouse model compared to other *Dyt1* cholinergic KO models is that there is preservation of both Dyt1 alleles in non-targeted cells (Liu et al., 2021) rather than KO of a single *Dyt1* allele throughout the whole body and KO of both *Dyt1* alleles in targeted cholinergic cells (Pappas et al., 2015, 2018). The inclusion of more affected cell types in the basal ganglia of D2KO mice aligns with our finding that D2KO mice had more severe deficits, including motor impairment and abnormal basal ganglia network activity during sensory-evoked fMRI compared to controls. The more limited effects observed in Ch2KO mice may be due to the more limited type and number of basal ganglia cells that are affected in this model, as striatal cholinergic interneurons account for less than 1% of all striatal neurons in rodents, whereas medium spiny neurons account for 97–98% of neurons in the rodent striatum (Oorschot, 2013). Although the basal ganglia is a critical hub in the pathophysiology of dystonia, Tor1A disruption in Ch2KO mice is not limited to striatal cholinergic neurons alone, and may impact cholinergic cells in the forebrain, midbrain, and spinal cord as observed in similar cholinergic KO models (Pappas et al., 2018). The BOLD signal reductions in the midbrain of Ch2KO mice may reflect disrupted cholinergic neuron populations in that region.

Network-level analyses revealed that D2KO mice had reduced sensory-evoked striatal functional connectivity to other regions within the striatum, globus pallidus, and portions of the sensorimotor cortex. In contrast, Ch2KO mice displayed elevated sensory-evoked striatal functional connectivity to the sensorimotor cortex and cerebellum. Taken together with prior findings of cortico-striatal hyper-connectivity in mice with conditional knock-out of *Dyt1* from forebrain cholinergic and GABAergic neurons (DeSimone et al., 2017), the present findings provide robust evidence that altered cortico-striatal connectivity is a hallmark of preclinical models of DYT1 dystonia. Aberrant functional connectivity has also been implicated in human populations with dystonia, particularly in sensorimotor networks of the cortex and basal ganglia (Corp et al., 2019; DeSimone et al., 2019). Similar to the increased functional connectivity between basal ganglia and cerebellum that we observed in Ch2KO mice, greater functional connectivity of the cerebellum has been associated with higher scores on the Unified Dystonia Rating Scale in patients with generalized dystonia (Okromelidze et al., 2020) and basal ganglia lesions that cause dystonia (Corp et al., 2019). It has been suggested that dystonia may be conceptualized as a functional network disorder, where there is disrupted flow and integration of signals across sensorimotor networks (Simonyan, 2018) and our present findings in the cortex, basal ganglia, and cerebellum support this body of evidence.

Concerning motor function, D2KO mice were quicker to fall during the rotarod task and had more slips during the beam-walking task compared to controls. In D2KO mice, a higher number of slips during beam-walking correlated with lower sensory-evoked BOLD signals in the basal ganglia and sensorimotor cortex, indicating that more severe motor deficits were observed in animals with less sensory system activation. We also found that longer rotarod latency-to-fall was correlated with lower inter-striatal functional connectivity in D2KO mice. Because D2KO mice had shorter latency-to-fall and lower inter-striatal functional connectivity compared to controls, the observed direction of this correlation may indicate that lower inter-striatal functional connectivity could be serving a compensatory function in the brains of D2KO mice. Regarding Ch2KO mice, we did not observe significant motor deficits at the ages used in this study. Prior work, however, showed that older Ch2KO mice eventually develop motor deficits in beam-walking and rotarod performance by 9 months of age (Liu et al., 2021). Although Ch2KO mice at the ages used in this study did not have significant motor deficits, we did observe a significant correlation where Ch2KO mice with greater functional connectivity between the striatum and cerebellum had shorter latency to fall during the rotarod task, suggesting that those mice with poorer motor performance showed more abnormal connectivity between striatum and cerebellum. This finding raises the possibility that similar patterns of abnormal connectivity between striatum and cerebellum may persist or become more prominent in Ch2KO mice that become symptomatic at older ages. Together these findings support a link between abnormal sensory-evoked network function and motor function in dystonia.

Striatal cholinergic interneurons are thought to play an important role in cortico-striatal plasticity (for a review, see Deffains and Bergman, 2015). Given that both D2KO and Ch2KO models have *Dyt1* disruption in striatal cholinergic interneurons, our findings of abnormal cortico-striatal functional connectivity in both models provide further support for the important role of striatal cholinergic interneurons in modulating input to the basal ganglia. In D2KO mice, the added impact of *Dyt1* conditional knock-out in additional cell types (*e.g.* dopamine-2 receptor expressing medium spiny neurons) appears to have a more profound impact on basal ganglia function and connectivity than *Dyt1* impairment of cholinergic neurons alone. Dopamine-2 receptors are thought to be essential in mediating the functional balance within the basal ganglia. Striatonigral neurons of the direct pathway contain bridging collateral fibers that allow for cross-talk with the indirect pathway *via* the globus pallidus, and these bridging collaterals are primarily regulated by dopamine-2 receptor activity (Cazorla et al., 2014). Our findings provide support for this notion by showing that D2KO mice compared to controls have more widespread reductions in sensory-evoked BOLD signal and more widespread alterations in striatal functional connectivity than did Ch2KO mice compared to controls.

In addition to indirect communication through the cortex, the basal ganglia and cerebellum communicate *via* the subthalamic nucleus, which is primarily considered to be a component of the indirect basal ganglia pathway and thus mediated by dopamine-2 receptor expressing medium spiny neurons (Bostan and Strick, 2018). Curiously, Ch2KO but not D2KO mice showed aberrant functional connectivity between the striatum and cerebellar cortex. Due to the inherent limitations of functional connectivity analysis, it is not possible to determine whether the increased functional connectivity between the striatum and cerebellar cortex in Ch2KO mice occurs through the subthalamic nucleus or thalamo-cortical intermediaries. Given that striatal cholinergic interneurons have been shown to mediate cortico-striatal plasticity (Calabresi et al., 2000), there is a basis for the involvement of the sensorimotor cortex in abnormal striatal-cerebellar functional connectivity in Ch2KO mice.

We did not detect microstructural differences in either D2KO or Ch2KO mice compared to controls using dMRI. Microstructural changes have been found with dMRI in other dystonia mouse models. Heterozygous *Dyt1* knock-in mice were shown to have reduced FA in the striatum and regions of the hindbrain (Uluğ et al., 2011) and heterozygous Dyt1 knock-out mice showed reduced FA in the sensorimotor cortex and brainstem (Vo et al., 2015). Both of these investigations were performed in animals with knock-in or knock-out of *Dyt1* effecting all

neurons in the brain, rather than only a subset of cell types. In addition, both investigations were performed with *ex vivo* dMRI, which permit longer scan times and higher spatial resolution. Most comparable to the present study, DeSimone et al. (2017) used *in vivo* dMRI and found altered microstructure in the striatum and cerebellum of Dlx-cKO mice, which have targeted *Dyt1* knock-out in forebrain cholinergic and GABAergic neurons. The Dlx-cKO mouse line used by DeSimone et al. (2017) display overt motor deficits by juvenile age (Pappas et al., 2015), therefore it is possible that the more severe and earlier appearing motor deficits in Dlx-cKO mice are reflected in microstructural changes detected with dMRI. Although both D2KO and Ch2KO models have been shown to have reduced density of striatal cholinergic interneurons (Liu et al., 2021; Yokoi et al., 2020), both show lower percentage reduction than do Dlx-cKO mice which have up to 60% reduced density of striatal cholinergic interneurons (Pappas et al., 2015). Striatal cholinergic interneurons account for less than 1% of all striatal neurons in rodents (Oorschot, 2013) and are localized at the borders between striosomal and matrix compartments which are distributed throughout the striatum (Crittenden and Graybiel, 2011). Since prior studies have linked diffusion imaging metrics to neurodegeneration and neuroinflammation (Chu et al., 2020; Febo et al., 2020), the current findings suggest that any subtle changes in neurodegeneration and neuroinflammation in D2KO and Ch2KO mice are not extensive enough to affect diffusion imaging metrics.

Investigating torsinA dysfunction in specific cell types is critical to understanding the complex pathophysiology of DYT1 dystonia. This study examined behavioral and neuroimaging outcomes in mice with targeted conditional knock-out of *Dyt1* in dopamine-2 receptor expressing neurons (D2KO) and cholinergic neurons (Ch2KO). We found that D2KO mice showed greater impairment than Ch2KO mice, including motor deficits, reduced sensory-evoked brain activity, and altered functional connectivity of the striatum that was correlated with motor deficits. These findings suggest that the added impact of torsinA dysfunction in dopamine-2 receptor medium spiny neurons and dopaminergic neurons of the basal ganglia generate more profound deficits than torsinA dysfunction of cholinergic neurons alone. Thus, disruption of cholinergic neurons alone did not elicit the degree of motor and brain impairments observed in DYT1 dystonia. Further studies will be needed to determine the precise mechanisms by which conditional knock-out of *Dyt1* in these cell types contribute to the unique patterns of basal ganglia activity and functional connectivity observed in D2KO and Ch2KO mice. Moreover, these findings suggest that sensory network dysfunction is correlated to motor deficits in dystonia. Sensory-evoked fMRI can be reliably measured in humans with similar equipment (Upadhyay et al., 2015) and may be a valuable research tool uncovering the link between sensory deficits and motor impairment in people with dystonia. The findings from this study have profound impacts on our understanding of the neurological mechanisms driving DYT1 dystonia and thus may inform future work towards a cure.

Declaration of Competing Interest

The authors report no conflict of interest or competing financial interests to disclose.

Acknowledgements

This work was supported by the National Institutes of Health (Project Number R01NS075012). A portion of this work was performed in the McKnight Brain Institute at the National High Magnetic Field Laboratory's Advanced Magnetic Resonance Imaging and Spectroscopy (AMRIS) Facility, which is supported by National Science Foundation Cooperative Agreement No. DMR-1644779 and the State of Florida. This work was also supported in part by an NIH award, S10RR025671, for MRI/S instrumentation.

References

Albanese, A., Bhatia, K., Bressman, S.B., DeLong, M.R., Fahn, S., Fung, V.S.C., Hallett, M., Jankovic, J., Jinnah, H.A., Klein, C., Lang, A.E., Mink, J.W., Teller, J.K., 2013. Phenomenology and classification of dystonia: a consensus update: dystonia: phenomenology and classification. Mov. Disord. 28, 863–873. https://doi.org/10.1002/mds.25475.

Asanuma, K., Ma, Y., Okulski, J., Dhawan, V., Chaly, T., Carbon, M., Bressman, S.B., Eidelberg, D., 2005. Decreased striatal D2 receptor binding in non-manifesting carriers of the DYT1 dystonia mutation. Neurology 64, 347–349. https://doi.org/10.1212/01.WNL.0000149764.34953.BF.

Avants, B.B., Yushkevich, P., Pluta, J., Minkoff, D., Korczykowski, M., Detre, J., Gee, J.C., 2010. The optimal template effect in hippocampus studies of diseased populations. Neuroimage 49, 2457–2466. https://doi.org/10.1016/j.neuroimage.2009.09.062.

Berman, B.D., Hallett, M., Herscovitch, P., Simonyan, K., 2013. Striatal dopaminergic dysfunction at rest and during task performance in writer's cramp. Brain 136, 3645–3658. https://doi.org/10.1093/brain/awt282.

Bostan, A.C., Strick, P.L., 2018. The basal ganglia and the cerebellum: nodes in an integrated network. Nat. Rev. Neurosci. 19, 338–350. https://doi.org/10.1038/s41583-018-0002-7.

Burciu, R.G., Hess, C.W., Coombes, S.A., Ofori, E., Shukla, P., Chung, J.W., McFarland, N. R., Wagle Shukla, A., Okun, M.S., Vaillancourt, D.E., 2017. Functional activity of the sensorimotor cortex and cerebellum relates to cervical dystonia symptoms. Hum. Brain Mapp. 38, 4563–4573. https://doi.org/10.1002/hbm.23684.

Calabresi, P., Centonze, D., Gubellini, P., Pisani, A., Bernardi, G., 2000. Acetylcholine-mediated modulation of striatal function. Trends Neurosci. 23, 120–126. https://doi.org/10.1016/S0166-2236(99)01501-5.

Carbon, M., Niethammer, M., Peng, S., Raymond, D., Dhawan, V., Chaly, T., Ma, Y., Bressman, S., Eidelberg, D., 2009. Abnormal striatal and thalamic dopamine neurotransmission: genotype-related features of dystonia. Neurology 72, 2097–2103. https://doi.org/10.1212/WNL.0b013e3181aa538f.

Cazorla, M., de Carvalho, F.D., Chohan, M.O., Shegda, M., Chuhma, N., Rayport, S., Ahmari, S.E., Moore, H., Kellendonk, C., 2014. Dopamine D2 receptors regulate the anatomical and functional balance of basal ganglia circuitry. Neuron 81, 153–164. https://doi.org/10.1016/j.neuron.2013.10.041.

Chu, W.T., DeSimone, J.C., Riffe, C.J., Liu, H., Chakrabarty, P., Giasson, B.I., Vedam-Mai, V., Vaillancourt, D.E., 2020. Alpha-synuclein induces progressive changes in brain microstructure and sensory-evoked brain function that precedes locomotor decline. J. Neurosci. https://doi.org/10.1523/JNEUROSCI.0189-20.2020.

Colon-Perez, L.M., Ibanez, K.R., Suarez, M., Torroella, K., Acuna, K., Ofori, E., Levites, Y., Vaillancourt, D.E., Golde, T.E., Chakrabarty, P., Febo, M., 2019. Neurite orientation dispersion and density imaging reveals white matter and hippocampal microstructure changes produced by Interleukin-6 in the TgCRND8 mouse model of amyloidosis. Neuroimage 202, 116138. https://doi.org/10.1016/j.neuroimage.2019.116138.

Corp, D.T., Joutsa, J., Darby, R.R., Delnooz, C.C.S., van de Warrenburg, B.P.C., Cooke, D., Prudente, C.N., Ren, J., Reich, M.M., Batla, A., Bhatia, K.P., Jinnah, H.A., Liu, H., Fox, M.D., 2019. Network localization of cervical dystonia based on causal brain lesions. Brain 142, 1660–1674. https://doi.org/10.1093/brain/awz112.

Cox, R.W., 1996. AFNI: software for analysis and visualization of functional magnetic resonance neuroimages. Comput. Biomed. Res. 29, 162–173. https://doi.org/10.1006/cbmr.1996.0014.

Crittenden, J.R., Graybiel, A.M., 2011. Basal Ganglia disorders associated with imbalances in the striatal striosome and matrix compartments. Front. Neuroanat. 5, 59. https://doi.org/10.3389/fnana.2011.00059.

Dang, M.T., Yokoi, F., McNaught, K.St.P., Jengelley, T.-A., Jackson, T., Li, J., Li, Y., 2005. Generation and characterization of Dyt1 ΔGAG knock-in mouse as a model for early-onset dystonia. Exp. Neurol. 196, 452–463. https://doi.org/10.1016/j.expneurol.2005.08.025.

Dang, M.T., Yokoi, F., Yin, H.H., Lovinger, D.M., Wang, Y., Li, Y., 2006. Disrupted motor learning and long-term synaptic plasticity in mice lacking NMDAR1 in the striatum. Proc. Natl. Acad. Sci. 103, 15254–15259. https://doi.org/10.1073/pnas.0601758103.

Dang, M.T., Yokoi, F., Cheetham, C.C., Lu, J., Vo, V., Lovinger, D.M., Li, Y., 2012. An anticholinergic reverses motor control and corticostriatal LTD deficits in Dyt1 ΔGAG knock-in mice. Behav. Brain Res. 226, 465–472. https://doi.org/10.1016/j.bbr.2011.10.002.

Deffains, M., Bergman, H., 2015. Striatal cholinergic interneurons and cortico-striatal synaptic plasticity in health and disease: Cholinergic Mechanisms of Movement Disorders. Mov. Disord. 30, 1014–1025. https://doi.org/10.1002/mds.26300.

DeSimone, J.C., Pappas, S.S., Febo, M., Burciu, R.G., Shukla, P., Colon-Perez, L.M., Dauer, W.T., Vaillancourt, D.E., 2017. Forebrain knock-out of torsinA reduces striatal free-water and impairs whole-brain functional connectivity in a symptomatic mouse model of DYT1 dystonia. Neurobiol. Dis. 106, 124–132. https://doi.org/10.1016/j.nbd.2017.06.015.

DeSimone, J.C., Archer, D.B., Vaillancourt, D.E., Wagle Shukla, A., 2019. Network-level connectivity is a critical feature distinguishing dystonic tremor and essential tremor. Brain 142, 1644–1659. https://doi.org/10.1093/brain/awz085.

Eskow Jaunarajs, K.L., Scarduzio, M., Ehrlich, M.E., McMahon, L.L., Standaert, D.G., 2019. Diverse mechanisms Lead to common dysfunction of striatal cholinergic interneurons in distinct genetic mouse models of dystonia. J. Neurosci. 39, 7195–7205. https://doi.org/10.1523/JNEUROSCI.0407-19.2019.

Febo, M., Perez, P.D., Ceballos-Diaz, C., Colon-Perez, L.M., Zeng, H., Ofori, E., Golde, T. E., Vaillancourt, D.E., Chakrabarty, P., 2020. Diffusion magnetic resonance imaging-derived free water detects neurodegenerative pattern induced by interferon-γ. Brain Struct. Funct. 225, 427–439. https://doi.org/10.1007/s00429-019-02017-1.

Hallett, M., 1995. Is dystonia a sensory disorder? Ann. Neurol. 38, 139–140. https://doi.org/10.1002/ana.410380203.
Kim, J., Yao, A., Atherley, R., Carstens, E., Jinks, S.L., Antognini, J.F., 2007. Neurons in the ventral spinal cord are more depressed by isoflurane, halothane, and propofol than are neurons in the dorsal spinal cord. Anesth. Analg. 105, 1020–1026 table of contents. https://doi.org/10.1213/01.ane.0000280483.17854.56.
Liu, Y., Xing, H., Sheng, W., Singh, K.N., Korkmaz, A.G., Comeau, C., Anika, M., Ernst, A., Yokoi, F., Vaillancourt, D.E., Frazier, C.J., Li, Y., 2021. Alteration of the cholinergic system and motor deficits in cholinergic neuron-specific Dyt1 knockout mice. Neurobiol. Dis. 105342 https://doi.org/10.1016/j.nbd.2021.105342.
Martella, G., Tassone, A., Sciamanna, G., Platania, P., Cuomo, D., Viscomi, M.T., Bonsi, P., Cacci, E., Biagioni, S., Usiello, A., Bernardi, G., Sharma, N., Standaert, D. G., Pisani, A., 2009. Impairment of bidirectional synaptic plasticity in the striatum of a mouse model of DYT1 dystonia: role of endogenous acetylcholine. Brain 132, 2336–2349. https://doi.org/10.1093/brain/awp194.
Martella, G., Maltese, M., Nisticò, R., Schirinzi, T., Madeo, G., Sciamanna, G., Ponterio, G., Tassone, A., Mandolesi, G., Vanni, V., Pignatelli, M., Bonsi, P., Pisani, A., 2014. Regional specificity of synaptic plasticity deficits in a knock-in mouse model of DYT1 dystonia. Neurobiol. Dis. 65, 124–132. https://doi.org/10.1016/j.nbd.2014.01.016.
Okromelidze, L., Tsuboi, T., Eisinger, R.S., Burns, M.R., Charbel, M., Rana, M., Grewal, S. S., Lu, C.-Q., Almeida, L., Foote, K.D., Okun, M.S., Middlebrooks, E.H., 2020. Functional and structural connectivity patterns associated with clinical outcomes in deep brain stimulation of the globus pallidus internus for generalized dystonia. AJNR Am. J. Neuroradiol. 41, 508–514. https://doi.org/10.3174/ajnr.A6429.
Oorschot, D.E., 2013. The percentage of interneurons in the dorsal striatum of the rat, cat, monkey and human: a critique of the evidence. Basal Ganglia 3, 19–24. https://doi.org/10.1016/j.baga.2012.11.001.
Ozelius, L.J., Hewett, J.W., Page, C.E., Bressman, S.B., Kramer, P.L., Shalish, C., de Leon, D., Brin, M.F., Raymond, D., Corey, D.P., Fahn, S., Risch, N.J., Buckler, A.J., Gusella, J.F., Breakefield, X.O., 1997. The early-onset torsion dystonia gene (DYT1) encodes an ATP-binding protein. Nat. Genet. 17, 40–48. https://doi.org/10.1038/ng0997-40.
Pappas, S.S., Darr, K., Holley, S.M., Cepeda, C., Mabrouk, O.S., Wong, J.-M.T., LeWitt, T. M., Paudel, R., Houlden, H., Kennedy, R.T., Levine, M.S., Dauer, W.T., 2015. Forebrain deletion of the dystonia protein torsinA causes dystonic-like movements and loss of striatal cholinergic neurons. eLife 4. https://doi.org/10.7554/eLife.08352.
Pappas, S.S., Li, J., LeWitt, T.M., Kim, J.-K., Monani, U.R., Dauer, W.T., 2018. A cell autonomous torsinA requirement for cholinergic neuron survival and motor control. Elife 7. https://doi.org/10.7554/eLife.36691.
Pisani, A., Martella, G., Tscherter, A., Bonsi, P., Sharma, N., Bernardi, G., Standaert, D.G., 2006. Altered responses to dopaminergic D2 receptor activation and N-type calcium currents in striatal cholinergic interneurons in a mouse model of DYT1 dystonia. Neurobiol. Dis. 24, 318–325. https://doi.org/10.1016/j.nbd.2006.07.006.
Quartarone, A., Hallett, M., 2013. Emerging concepts in the physiological basis of dystonia. Mov. Disord. 28, 958–967. https://doi.org/10.1002/mds.25532.
Richter, F., Klein, L., Helmschrodt, C., Richter, A., 2019. Subtle changes in striatal muscarinic M1 and M4 receptor expression in the DYT1 knock-in mouse model of dystonia. PLoS One 14, e0226080. https://doi.org/10.1371/journal.pone.0226080.
Scarduzio, M., Zimmerman, C.N., Jaunarajs, K.L., Wang, Q., Standaert, D.G., McMahon, L.L., 2017. Strength of cholinergic tone dictates the polarity of dopamine D2 receptor modulation of striatal cholinergic interneuron excitability in DYT1 dystonia. Exp. Neurol. 295, 162–175. https://doi.org/10.1016/j.expneurol.2017.06.005.
Sciamanna, G., Tassone, A., Martella, G., Mandolesi, G., Puglisi, F., Cuomo, D., Madeo, G., Ponterio, G., Standaert, D.G., Bonsi, P., Pisani, A., 2011. Developmental profile of the aberrant dopamine D2 receptor response in striatal cholinergic interneurons in DYT1 dystonia. PLoS One 6, e24261. https://doi.org/10.1371/journal.pone.0024261.
Sciamanna, G., Hollis, R., Ball, C., Martella, G., Tassone, A., Marshall, A., Parsons, D., Li, X., Yokoi, F., Zhang, L., Li, Y., Pisani, A., Standaert, D.G., 2012. Cholinergic dysregulation produced by selective inactivation of the dystonia-associated protein torsinA. Neurobiol. Dis. 47, 416–427. https://doi.org/10.1016/j.nbd.2012.04.015.
Simonyan, K., 2018. Neuroimaging applications in dystonia. Int. Rev. Neurobiol. 143, 1–30. https://doi.org/10.1016/bs.irn.2018.09.007.
Simonyan, K., Berman, B.D., Herscovitch, P., Hallett, M., 2013. Abnormal striatal dopaminergic neurotransmission during rest and task production in spasmodic dysphonia. J. Neurosci. 33, 14705–14714. https://doi.org/10.1523/JNEUROSCI.0407-13.2013.
Smith, S.M., Nichols, T.E., 2009. Threshold-free cluster enhancement: addressing problems of smoothing, threshold dependence and localisation in cluster inference. Neuroimage 44, 83–98. https://doi.org/10.1016/j.neuroimage.2008.03.061.
Uluğ, A.M., Vo, A., Argyelan, M., Tanabe, L., Schiffer, W.K., Dewey, S., Dauer, W.T., Eidelberg, D., 2011. Cerebellothalamocortical pathway abnormalities in torsinA DYT1 knock-in mice. Proc. Natl. Acad. Sci. U. S. A. 108, 6638–6643. https://doi.org/10.1073/pnas.1016445108.
Upadhyay, J., Lemme, J., Anderson, J., Bleakman, D., Large, T., Evelhoch, J.L., Hargreaves, R., Borsook, D., Becerra, L., 2015. Test-retest reliability of evoked heat stimulation BOLD fMRI. J. Neurosci. Methods 253, 38–46. https://doi.org/10.1016/j.jneumeth.2015.06.001.
Vo, A., Sako, W., Dewey, S.L., Eidelberg, D., Uluğ, A.M., 2015. 18FDG-microPET and MR DTI findings in Tor1a+/− heterozygous knock-out mice. Neurobiol. Dis. 73, 399–406. https://doi.org/10.1016/j.nbd.2014.10.020.
Yokoi, F., Dang, M.T., Li, J., Standaert, D.G., Li, Y., 2011. Motor deficits and decreased striatal dopamine receptor 2 binding activity in the striatum-specific Dyt1 conditional knockout mice. PLoS One 6, e24539. https://doi.org/10.1371/journal.pone.0024539.
Yokoi, F., Oleas, J., Xing, H., Liu, Y., Dexter, K.M., Misztal, C., Gerard, M., Efimenko, I., Lynch, P., Villanueva, M., Alsina, R., Krishnaswamy, S., Vaillancourt, D.E., Li, Y., 2020. Decreased number of striatal cholinergic interneurons and motor deficits in dopamine receptor 2-expressing-cell-specific Dyt1 conditional knockout mice. Neurobiol. Dis. 134, 104638. https://doi.org/10.1016/j.nbd.2019.104638.